

Sublimed fine-grained dysprosium: Significant magnetocaloric effect

Yu.S. Koshkidko^{a,*}, J. Cwik^a, C. Salazar Mejia^b, N.A. Dormidontov^c, P.A. Prokofev^c,
A.S. Bakulina^c, A.A. Nikitin^d, A.A. Khomich^d, R.R. Gimaev^e, A.S. Andreenko^e, Zh.P. Burmii^f,
A.A. Telitsa^e, V.I. Zverev^e, N.B. Kolchugina^c

^a Institute of Low Temperature and Structure Research, Polish Academy of Sciences, Wrocław 50-422, Poland

^b Hochfeld-Magnetlabor Dresden (HLD-EMFL), Helmholtz-Zentrum Dresden-Rossendorf, 01328 Dresden, Germany

^c Baikov Institute of Metallurgy and Materials Sciences, Russian Academy of Sciences, Leninskii Pr. 49, Moscow, 119334 Russia

^d National Research Center Kurchatov Institute, Pl. Akademika Kurchatova 1, Moscow, 123182 Russia

^e Moscow State University, Faculty of Physics, Leninskie Gory 1, Moscow, Russia

^f Institute of Microelectronics Technology and High-Purity Materials, Russian Academy of Sciences, Chernogolovka, Russia

ARTICLE INFO

Handling Editor: Prof. L.G. Hultman

Keywords:

Vacuum sublimation
High-purity dy
Fine-grained structure
Atom probe tomography
Magnetocaloric effect
Magnetization
Pulsed magnetic fields

ABSTRACT

As is known, rare-earth metals (REMs) are promising magnetocaloric materials. The magnitude of the magnetocaloric effect (MCE) of REMs significantly depends on their purity. This paper presents results of studies of the magnetic and magnetocaloric properties of sublimed dysprosium, prepared in the course of the present study, with an emphasis on its impurity and structure perfection. The comprehensive analysis of the chemical composition of sublimed dysprosium, which was performed for the first time by atom probe tomography, showed that the metal corresponds to high-purity rare-earth metals (3 N+). The MCE effect was studied using direct measurements of the adiabatic temperature change (ΔT_{ad}) in pulsed (up to 50 T) and steady (up to 14 T) magnetic fields. The studies of the MCE of polycrystalline sublimed Dy by direct method showed that the high ΔT_{ad} value for sublimed Dy are comparable with those obtained for single-crystal Dy in magnetic fields up to 5 T. The vacuum sublimation, which is more economical and technologically advanced in contrast to single crystal growing, can be used to create magnetocaloric REM-based materials with high MCE values.

1. Introduction

Magnetocaloric effect (MCE) is the magnetic material temperature change in an external magnetic field. As the physical quantity, the MCE can be evaluated via the isothermal magnetic entropy change, ΔS_{mag} , under isothermal conditions and the adiabatic temperature change, ΔT_{ad} , under adiabatic conditions, which take place with changing an applied magnetic field. Traditional ferromagnetic and antiferromagnetic materials exhibit the maximum magnetocaloric effect near the Curie, T_C , and Néel, T_N , temperatures, which correspond to the most fast-changing magnetization as a function of temperature.

Approaches to a fundamentally new technology of solid-state magnetic cooling (SMC) at room and cryogenic temperatures can be developed based on MCE [1–5]. Thus, magnetic materials exhibiting high MCE value are of the great interest for researchers nowadays.

Heavy rare-earth metals (REMs), being the unending source for researching magnetic phenomena and magnetic field-induced effects

which could be used in practice, are one of the promising magnetocaloric materials for the magnetic cooling technology. This is due to the high magnetic moment of REMs and the fact that their magnetic phase transformation temperatures cover the range from cryogenic to room temperatures. In recent years, the understanding of REM physical properties in the vicinity of magnetic and structural transformation temperatures has advanced significantly [3–5]. The most important factor to have high MCE values in RE metals is their purity [6–8].

Dysprosium exhibits various types of magnetic ordering. Its temperature- and field-induced transformations of the magnetic order and manifestation of MCE were actively studied for several decades using Dy samples differing in purity, structural state, and structure perfection [7, 9,10]. Dysprosium exhibits both heating and cooling upon adiabatic magnetization depending on its magnetic state (ferromagnetic, paramagnetic, or antiferromagnetic) and a change in state is reflected by its magnetocaloric behavior. In numerous studies, the magnetocaloric effect has been correlated with temperature, pressure, magnetization, and

* Corresponding author.

E-mail address: y.koshkidko@intibs.pl (Yu.S. Koshkidko).

<https://doi.org/10.1016/j.vacuum.2024.113239>

Received 21 December 2023; Received in revised form 20 April 2024; Accepted 21 April 2024

Available online 23 April 2024

0042-207X/© 2024 Elsevier Ltd. All rights reserved.

magnetic field intensity [6,11–17].

In zero magnetic field, Dy is paramagnetic above its Néel temperature (T_N) equal to 179 K [16]; below the Néel temperature, the helical antiferromagnetic phase with a basal-plane spiral structure exists. As was shown in earlier studies [18–20], this transformation is accompanied by orthorhombic distortions of the hexagonal close-packed structure of the metal. As temperature decreases, the helical antiferromagnetic (AFM) phase remains stable down to the Curie temperature 89 K [16]. Below the Curie temperature, the metal is ferromagnetically ordered to 4.2 K. In the ferromagnetic (FM) phase, the easy magnetization direction coincides with the a axis. The transformation occurred at the Curie temperature in zero magnetic field is of the first-order [15], while the one at the Néel temperature is of the first-order or second-order transformation [14]. In the later study, a number of arguments in favor of the second-order transition in Dy at the Néel temperature are reported and discussed.

The field-induced magnetic phase transformations in the temperature range of magnetic state of Dy, namely, the field - temperature magnetic phase diagrams were designed in Refs. [8,10,14,15,21,22], which allow us to trace the evolution of the diagrams with changing purity of the metal and its structure perfection.

In [21], a magnetic phase diagram of Dy is presented. The temperature range between T_C and T_N is of special interest, because here magnetic phase transitions can be induced by an applied magnetic field, and phase transitions from the helical AFM to the ferromagnetic and to the fan state, respectively from the fan to the ferromagnetic state take place. The intermediate fan magnetic structure appears between the AFM and FM phases in a certain range of nonzero magnetic fields between ~ 127 and ~ 179 K. No indication for the field dependence of the transition temperature T_N was obtained. The purity of Dy sample is not specified.

In [14], the magnetic phase diagram of Dy was improved (based on magnetocaloric data) and two new magnetic phases were identified using high-purity Dy single crystal. The reached adiabatic temperature change did not exceed 1.5 K at 93 K and 2.5 K at 121 K in fields of to 10 kOe. The same values of the adiabatic temperature change are reported in Ref. [8], in which the H-T phase diagram of Dy was revised to reflect the presence of two unknown magnetic phases existing between ~ 105 and ~ 127 K in the magnetic fields ~ 3 to 6 kOe and between ~ 179 and ~ 182 K in magnetic fields 8–12 kOe.

In [8], the magnetocaloric effect, magnetization, ac magnetic susceptibility, and heat capacity of high-purity single crystals of dysprosium have been investigated over wide temperature and magnetic field ranges with the magnetic field applied in parallel to either the a or c axes of the crystal. Notable differences in the behavior of the physical properties when compared to Dy samples studied in the past have been observed between 110 and 125 K, and between 178 and ~ 210 K. The reduction of MCE of relatively impure Dy samples near the Néel temperature was explained by the formation of antiferromagnetic clusters in these samples. Dysprosium is a classic example of a system where magnetic and crystallographic sublattices can be either coupled or decoupled from one another. The effect of commensurability of the crystal and magnetic sublattices on the magnetic phase diagram was studied experimentally and theoretically. The presence of newly found anomalies in the physical properties has been considered as evidence of previously unreported states of Dy. The refined magnetic phase diagram of dysprosium with the magnetic field vector parallel to the a axis of a crystal has been constructed and discussed.

We failed to find information about the magnetocaloric effect of Dy measured in high pulsed magnetic fields. According to theoretical predictions in Ref. [23] the value of MCE in fields of ~ 1 T is lower than 1 K, whereas, in higher and ultrahigh pulsed magnetic fields of ~ 10 – 10^3 T using pulses of 10^{-4} – 10^{-5} s in duration, the MCE can reach $\sim 10^2$ K.

As is known, it is an extremely difficult and complex problem to prepare ultra-high purity rare earth metals, and even trace impurities at ppm or sub-ppm level, in particular the interstitial impurities, can

substantially affect the physical and chemical properties of REMs [24] and the temperatures of magnetic phase transitions and their completeness.

Many studies were performed to understand the formation of impurity composition of distilled and sublimed rare-earth metals in the course of purification processes. In Ref. [25], distribution rules of impurity contents in distilled metallic dysprosium were studied, and a theoretical analysis was carried out for Al and Fe impurities. The physical process of the distillation was shown to be coincident substantially with that of the solidification. The diffusion of impurity in liquid metal could reach a quasi-equilibrium state; at the latter stage of distillation process, the diffusion rate of impurity in liquid metal is decreased, and the impurity content in distilled metal was higher. It is possible to assume that the diffusion of impurities in the metal deposited in solid is not high and a REM metal prepared by solid-state sublimation and subsequent deposition in solid can be characterized by the higher purity.

The behavior gaseous impurities, in particular, oxygen in the course of sublimation-distillation process of REMs is of special interest since oxygen is major gaseous impurity because the starting materials are REM oxides that were subjected to fluoridation. In Refs. [26,27], to decrease the impurity content in Tb and Gd, a two-step approach was employed; the approach consists in combining the traditional vacuum distillation method with an active metal (Ca) external suction method. The behavior of a number of metallic impurities formed complex oxides was demonstrated and their location in the distilled metal was revealed. The behavior of oxygen and nitrogen during distillation by an example of Tb was studied in Ref. [28]. It was shown that the oxygen concentration in distillate presents exponentially increasing tendency. At the same time, the behavior of impurity fluorine in the course of distillation were not studied.

With a focus on the purity of Dy, which was prepared by two-fold vacuum sublimation, we undertook a detailed study of the MCE of the material. To find common trends in the behavior of MCE, it was measured in high steady and pulsed magnetic fields. We used Dy, the structure and impurity homogeneity of which was characterized at both micro- and nano-scale levels.

2. Experimental

In the present study, as the base physical-chemical preparation method of pure Dy, we use vacuum sublimation [29]. Based on preliminary analysis of the behavior and distribution of impurities, in the course of vacuum sublimation of Dy, we elaborated optimum conditions for the preparation of high-purity Dy. According to preliminary calculated data [29], the sublimation process of Dy is efficient for removing both metallic and interstitial impurities since the main impurities present in Dy, according to their vapor pressures, are removed either at the beginning stage of the sublimation process or remain in the crucible and evaporate at the final stage.

The main impurities in commercial Dy (DyM-1) are Fe, Al, Cu, Si, Cl, accompanying REMs (0.1 wt %), and Ca, F, Ta, La (that are manufacturing impurities). Interstitial (gas-forming impurities (O, N, H, C)) in REMs and, in particular, in Dy can be inherited from minerals (ores), enter in the manufacturing process, and result from the high chemical reactivity of REMs.

The vacuum sublimation process is fulfilled at the Baikov Institute of Metallurgy and Materials Science, Russian Academy of Sciences using a resistance furnace equipped with a tantalum crucible (evaporator) containing commercial Dy and water-cooled cone-shaped copper condenser to collect the sublimed Dy. In the course of sublimation, a dynamic vacuum was maintained; the residual gas pressure was about $1.5 \cdot 10^{-4}$ Pa. The sublimation (evaporation from solid) and condensation temperatures correspond to deposition of metal in solid. The two-fold sublimation process was performed.

The impurity composition of Dy druse consisting of closely growing

crystals was determined by mass-spectrometry using a X Series 7 (Thermo Fisher Scientific, U.S.A.) quadrupole inductively-coupled plasma spectrometer. The contents of impurity oxygen and nitrogen were determined using a TC-436 analyzer (LECO, U.S.A.).

The structure of sublimed Dy sample and its impurity-element composition were studied by scanning electron microscopy (SEM) using a COXEM-EM30 (Daejeon, Korea) scanning electron microscope equipped with an Energy-dispersive X-ray spectroscopy analyzer (EDS, Oxford instruments, Oxford, UK).

Atomic force microscopy of the Dy section was performed in a semi-contact mode using a Multimode Nanoscope III (Veeco) atomic-force microscope.

3D distribution of the atomic species in dysprosium crystallites was studied by atom probe tomography performed at the National Research Center Kurchatov Institute using an APPLE-3D microscope [30]. Tomographic atom probe microscopy complements other existing techniques of material microstructure and elemental analysis and provides more information about the features detected at the sub-nanoscale range. The sensitivity of the method makes it possible to register impurities with a content of 10–50 atoms per million. Samples for the atom probe tomography were prepared on an FEI Quanta 3D dual-beam system using focused ion beam (FIB) lift-out techniques [31].

The texture of high-purity Dy druse was studied and the crystallographic orientations of crystallites comprising it were determined. For the texture studies, the druse was cut along the deposition direction (axial direction). The texture was determined based on four incomplete direct pole figures {00.4}, {10.2}, {10.3}, and {11.0} that were taken under reflection mode conditions using a DRON-7 diffractometer (St. Petersburg, Russia) and CoK_{α} radiation. The tilting α and azimuthal β angles ranged from 0 to 70° and 0 to 360° at a step of 5° were used [32, 33], respectively. The orientation distribution function (ODF) was calculated using measured pole figures. The volume fractions of orientations W_i were improved using TeXXor software [34–36].

We carried out magnetization measurements in a Physical Property Measurement System with VSM option (PPMS, Quantum Design).

To study the MCE by direct method in steady magnetic fields, an experimental device was used, which allowed one to perform the direct MCE measurements in magnetic fields of up to 14 T in a temperature range of 4.2–350 K using the extraction method and a Bitter-type magnet generated the steady magnetic field. Both the temperature of the sample and the temperature change (due to the MCE) were measured using a differential thermocouple [37].

The MCE effect of sublimed Dy was also measured by direct method in pulsed magnetic fields of up to 50 T using micro thermocouples. The measurements were performed in the Dresden high-magnetic field laboratory (HLD-EMFL), Helmholtz-Zentrum Dresden-Rosendorf. The fast field sweep (to 1500 T/s) during a pulse allows one to keep the adiabatic conditions while measuring the temperature change of a sample in the course of its magnetization [38]. In this case, to obtain the adiabatic conditions, the fast magnetization of sample is realized at the expense of fast magnetic-field switching on.

3. Results and discussion

3.1. Impurity composition, microstructure, and texture of sublimed Dy

The impurity composition of sublimed Dy is given in Table 1.

The contents of the other impurity elements, in particular, iron is

below the detection limit (0.1 ppm). Without taking into account the gas-forming element contents, the content of the matrix element (Dy) is no less than 99.96 wt %. Thus, according to the analysis data, the purity of the sublimed Dy is 3 N; this metal corresponds to the high-purity grade of rare-earth metals.

The microstructure of sublimed Dy is represented by coarse extended crystallites. The ratio of crystallite sides is ~ 1.4 , and the length of crystallites is in a range of 200–700 μm (see Fig. 1a and b). Dark inclusions are observed mainly at crystallite boundaries. The local chemical analysis showed that the inclusions can be either dysprosium fluoride or dysprosium oxides (Fig. 1b, c, d Tables 2 and 3). The fluoride and oxide inclusions are $\sim 10 \mu\text{m}$ in size (Fig. 1d). The chemical etching allowed us to reveal fine grains within the crystallites, which are 200–800 nm in size (see Fig. 2a and b). It should be noted that the etching occurs mainly along certain directions; this fact indicates that a crystallite is a packet comprising fine grains characterized by a low misorientation angle (Fig. 3a and b). Results of atomic-force microscopic studies confirm the presence of impurities segregated at grain boundaries of coarse crystallites (Fig. 4a). Oriented structures (Fig. 4b) are observed, which are similar to those observed in Fig. 3a and b. Because of the high reactivity of the metal, an oxide film in the form of islands forms. This fact substantially makes difficult the visualization of nano-sized grains within a crystallite. An Atomic force microscopy image given in Fig. 4c shows the structure characterized by fine grains.

The presence of oxide inclusions in distilled Tb and Gd was demonstrated in Refs. [26,27]. In this study, inclusions of impurity element oxides were detected. In our study, Dy oxide and fluoride inclusions were found. This fact allows us to infer a conclusion about the behavior of impurity fluorine in the course of distillation and sublimation of REMs. It is likely that fluorine is present in the distillate and is difficult to be extracted from REMs by vacuum distillation.

According to the textural analysis data, no primary orientation of crystallites comprising the druse is observed. Fig. 5 shows sections of ODF for Eulerian angle φ_2 for the axial plane of sample. The base orientations of crystallites and their volume fractions are given in Fig. 5 and Table 4.

As is seen, the disperse multicomponent texture is formed. In this case, the fraction of texture-less component is sufficiently high and equal to 0.67. This means that 67 % crystallites are randomly oriented with respect to the external coordinate system. Fig. 6 shows direct pole figures (00.4) and (11.0) constructed from ODFs.

Pole figures show that the total orientation direction of crystallites makes an angle of $\sim 30^\circ$ (anticlockwise) with the axial direction of sample.

To perform atom probe tomographic studies of sublimed Dy, individual crystallites were separated from the druse.

For atom probe analysis, specimens were lifted out from different places of the druse, corresponding to the beginning and end stages of the sublimation process. Typical signals on mass spectrum obtained are shown in Fig. 7. During the evaporation of the material, Dy^+ ions with charge states of +1, +2, +3 and several impurities, such as C, P, Fe were detected. In addition, signals corresponding to the molecular ions DyO^+ , and Dy(OH)_2^+ , DyF_3^{2+} were registered. Also small amount of Ho^+ atoms was registered. Signal from ^{69}Ga results from the specimen preparation and was excluded from the final chemical composition evaluation. Estimated chemical composition of the specimens is represented in Table 5. Molecular ions were separated and counted as individual atoms. Atomic maps of the samples are shown in Fig. 8. Also in Fig. 8, the high

Table 1
Content of base impurities in Dy subjected to two-fold sublimation.

Impurity content, ppm wt										
Cu	Y	La	Ce	Pr	Nd	Sm	Gd	Pb	O	N
18.6	13.3	5.1	1.3	0.89	25.6	0.64	6.0	7.5	245	5.3

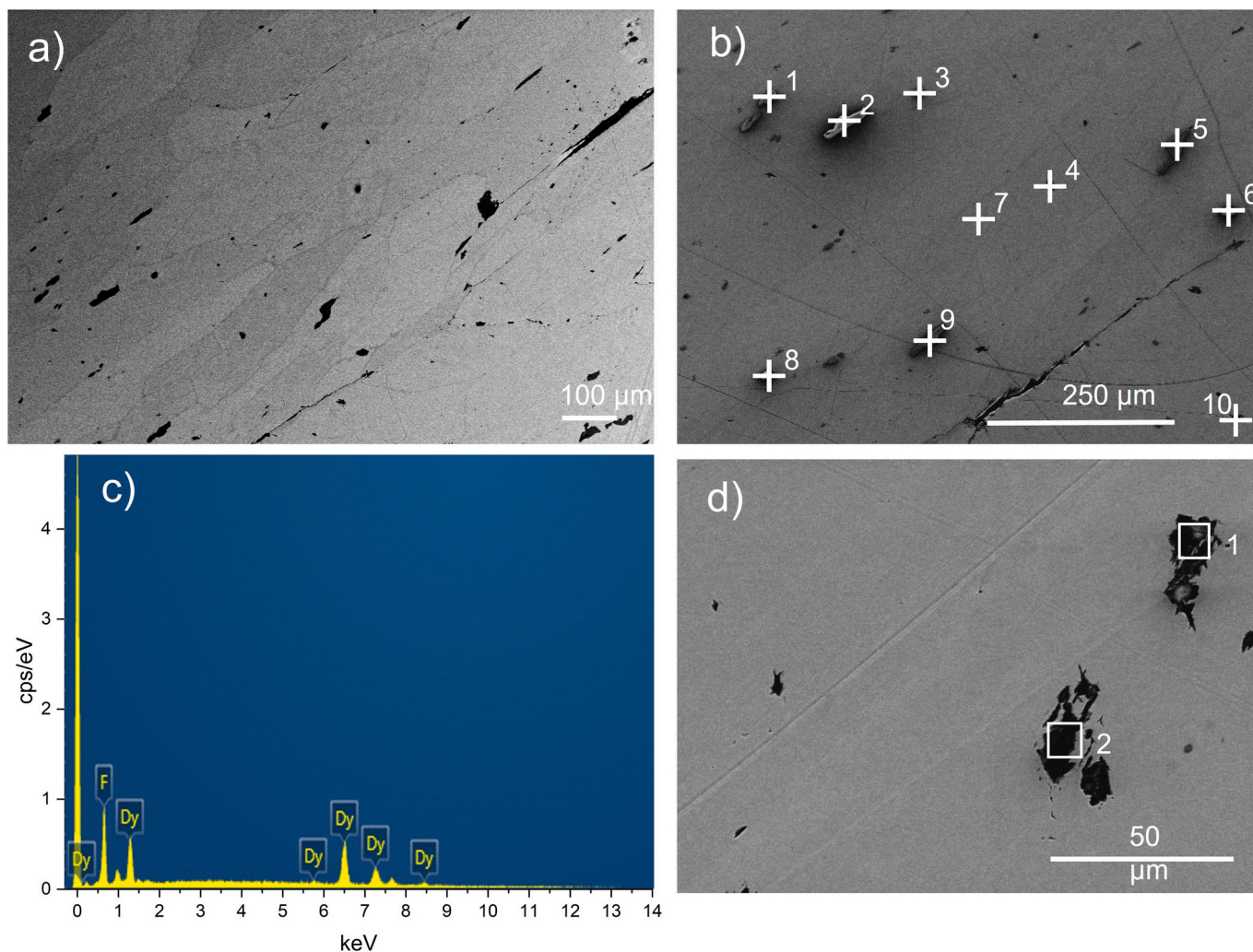


Fig. 1. (a) SEM image of the microstructure of sublimed Dy. (b) SEM image of sublimed Dy. Points of local electron microprobe analysis (energy dispersive spectroscopy) are shown. Chemical composition of marked areas is represented in Table 2. (c) Spectrum corresponding to an area 2 shown in Fig. 1b. (d) Black areas correspond to dysprosium oxide inclusions (for chemical composition see Table 3).

Table 2

Chemical composition (at %) of local areas at the Dy surface.

Spectrum ^a	Dy	F	Si	O
1	36.7	61.3	1.9	
2	35.6	64.4		
3	38.0	62.0		
4	91.3			
5	75.5	24.5		
6	42.9	55.2	2.0	
7	100.0			
8	40.6	59.4		8.7
9	43.7	56.3		
10	100.0			

^a Spectra numbers are given in Fig. 1b.

Table 3

Chemical composition (at %) of inclusions (Fig. 1d) observed at the Dy sample surface.

Spectrum	Dy	F	Si	O
1	42.1	–	11.6	46.3
2	40.9	–	14.2	44.9

contrast of dysprosium atoms is due to its grain microstructure, since more intensive evaporation of atoms occurs at the crystallite boundaries. A non-uniform distribution of fluorine and holmium atoms was found. We assume that fluorine atoms partially remaining in the material matrix form nanosized clusters. Fig. 9 shows isosurface plotted around F-enriched nanograin. This cluster is enriched in F and Ho atoms by 3.9 and 0.8 at.% correspondingly. Its diameter is approximately 9 nm.

The data obtained allow us to detect the presence of impurities in the form of layers in the sublimed metal, which are enriched in a certain impurity at the nanoscale. This fact is likely to reflect the evaporation process in accordance with the vapor pressure of the elements. The Dy content in the samples prepared in the form of 100-nm needles was determined to be 99.4 and 97.83 at %. Correlations in the arrangement of layers are observed. To explain the results obtained for impurity composition and impurity distribution in the sublimed metal, additional studies should be performed. Nevertheless, the atom probe tomography has demonstrated to be useful for the characterization of the impurity composition of REMs. The impurity composition of sublimed Dy and the inhomogeneous distribution of impurities allow us to state the specific impurity composition of sublimed Dy and to define it as the high-purity metal.

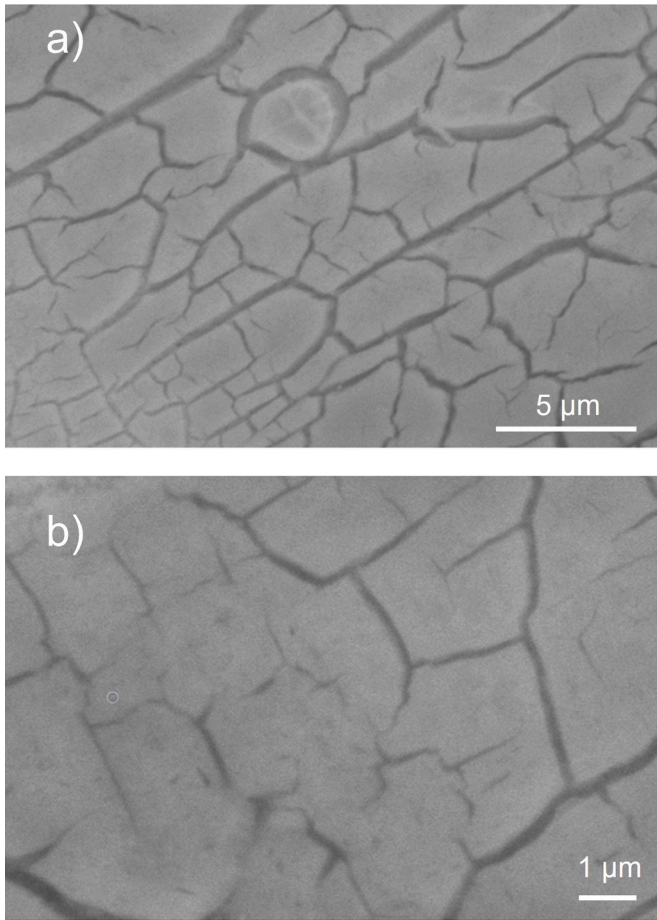


Fig. 2. (a, b) SEM image of the microstructure of sublimed Dy taken with different magnifications; fine grains are observed.

3.2. Magnetic and magnetocaloric properties of sublimed fine-grained Dy in high magnetic fields

Fig. 10 shows temperature dependences of the magnetization of sublimed Dy measured under zero-field cooling and field cooling (ZFC and FC, respectively) conditions. As is seen, upon heating (ZFC), the abrupt decrease in the magnetization take place near the Curie temperature, which corresponds to FM-AFM transition. The further heating leads to the maximum related to the Néel temperature corresponding to the AFM-PM phase transition. The determined magnetic phase transition temperatures agree well with those available in the literature [8].

Fig. 11 shows the field dependences of the magnetization. The dependences measured at 150-178 K exhibit anomalies (inflections) related to the field-induced AFM-fan-FM transition [8,10]. Neutron diffraction studies [39,40] indicated that, in the temperature range between 87 and 179 K, the helix AFM ordering occurs. In the initial part of the magnetization curve, the magnetic field leads to a slight distortion of the spiral AFM structure, which forces the magnetic moments to revolve by a small angle to the field direction; in this case, the magnetization value slightly depends on the field [39]. At a critical value of the field, which, according to the phase diagram [8], depends on temperature, the transition from the distorted AFM structure to the fan AFM structure takes place. In the course of subsequent increase in the magnetic field, all magnetic moments become arranged in parallel to the field (see **Fig. 11**).

As was noted above, Dy exhibits high MCE [6,8–10,17,41]. Methods for the study and estimation of the MCE can be divided into direct and indirect [7,41]. In the present study, the isothermal entropy change (ΔS_{iso}) is calculated from magnetization data (indirect method) and the

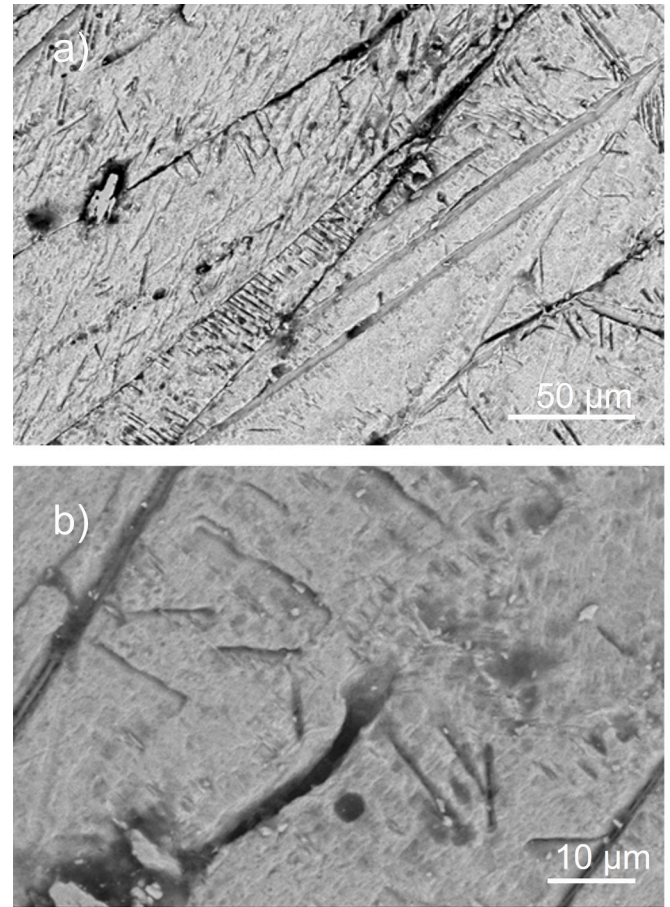


Fig. 3. (a, b) SEM image (taken with different magnifications) of the etched surface of sublimed fine-grained Dy; etching along crystallographic directions takes place.

adiabatic temperature change was measured directly. The isothermal entropy change as a function of both temperature and magnetic field change was determined from magnetization isotherms (**Fig. 11**) using the thermodynamic Maxwell relation:

$$\Delta S_{iso} = \int_0^H \left(\frac{\partial M(T, H)}{\partial T} \right)_H dH, \quad (1)$$

where $M(T, H)$ is magnetization M as a function of magnetic field H and absolute temperature T [1,2].

As is seen from the temperature dependences of the isothermal entropy change (**Fig. 12**), a maximum is observed near the Néel temperature for all values of magnetic fields. The maximum value observed is 32 J/(kgK) at 180 K for a field change of 14 T.

A distinctive feature of the temperature dependences of the isothermal entropy change is the existence of inverse MCE in moderate fields up to 2 T in the range of AFM ordering (see phase diagram [8]). The existence of the inverse MCE in moderate magnetic fields can be also observed in the temperature dependences of ΔT_{ad} (**Fig. 13**). As the field increases to 5 T, the effect of inverse MCE on the total MCE almost disappears. The further increase in the magnetic field leads to the fact that the total MCE mainly is determined by direct MCE of the forced magnetization.

The maximum adiabatic temperature change, $\Delta T_{ad} = 21$ K, is observed at 179 K for a steady magnetic field of 14 T. This value agrees well with that, 22.6 K, obtained in measuring the MCE in the pulsed magnetic fields (**Fig. 13**, open symbols). A slight difference (1.6 K) is due to the difference in the degree of approaching to the adiabatic conditions

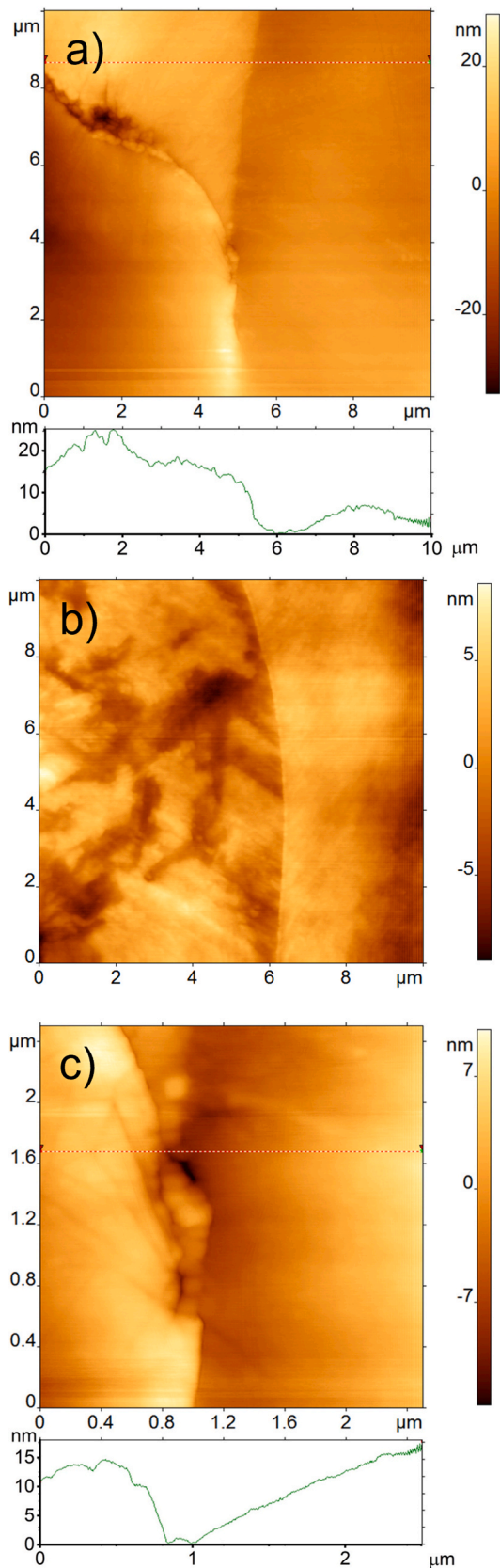


Fig. 4. Atomic force microscopy image of sublimed Dy: (a) impurity segregations at crystallite grain boundaries and (b, c) fine grains comprising crystallites. Images below Fig. (a) and (c) show the surface profile measured along the dotted line in the main image.

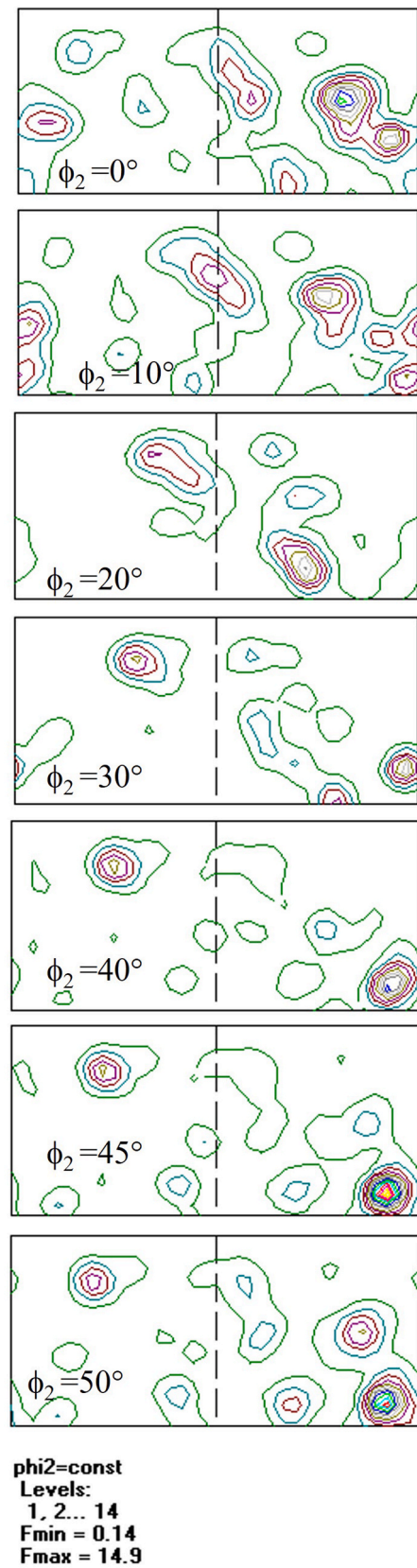
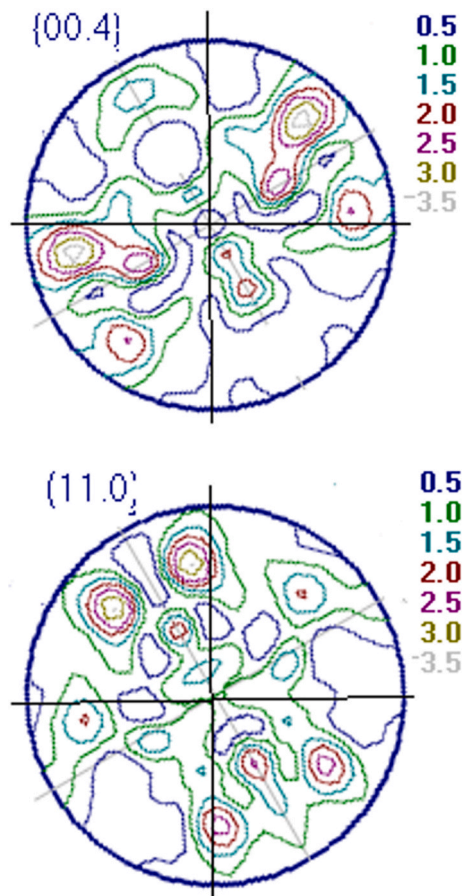
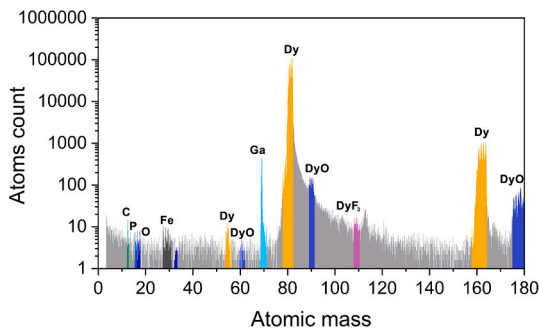


Fig. 5. ODF for the axial plane of sublimed Dy. Maximum and minimum values of ODF and their levels are shown.

Table 4

Base orientations and their volume fractions for the axial plane of Dy sample.

(hkl)<uvw>	Eulerian angle			Volume fraction
	φ_1	Φ	φ_2	
(38.-11.4)<-8632>	165	79	45	0.07
(-12-13)<-3-252>	146	45	0	0.05
(-24-23)<-9-1.10.2>	168	64	0	0.04
(-2.11.-95)<-5057>	130	74	20	0.04
(14.-5.21)<5-832>	45	22	40	0.03
(07-74)<-2-110>	174	73	30	0.03
(-12-13)<2.-11.9.11>	105	45	0	0.02
(-12-12)<15.-2.13.3>	13	57	0	0.02
(-12-15)<2-533>	97	32	0	0.01
(-7.14.-72)<-6-17.10>	122	85	0	0.01
(01-10)<-4223>	143	90	30	0.01
Texture-less component				0.67

**Fig. 6.** Direct pole figures (00.4) and (11.0) for the axial plane of sublimed Dy.**Fig. 7.** Mass spectrum acquired by atom probe tomography.

in measuring the temperature upon magnetization of sample. In the case of steady measurement, the maximum field is reached in 1 s. In the case of pulsed field, this time is 13 ms. Therefore, when measuring in steady magnetic fields, the relatively small part of ΔT_{ad} can be lost as a result of heat exchange between the sample and environment. According to our estimations, these losses are 7 % of the maximum value of ΔT_{ad} .

In turn, the maximum value of ΔT_{ad} observed in a pulsed magnetic field of 50 T is 51 K (Fig. 14). The value of ΔT_{ad} in this field becomes comparable with that of Gd ($\Delta T_{ad} = 52$ K in a field of 50 T [42]). Earlier [11], the ultimate value of ΔT_{ad} in ultrahigh magnetic fields (above ~600 T) was predicted for a number of REMs. For Dy and Gd, the ultimate value of ΔT_{ad} at the magnetic phase transformation temperature according to the mean-field model (T_N for Dy and T_C for Gd) is 231 K and 235 K, respectively [11]. According to such modelling predictions, the maximum in the temperature dependence of ΔT_{ad} in the magnetic phase transition region disappears in a field of more than 200 T [11,12].

The similar behavior can be observed in the experimental temperature-dependence ΔT_{ad} measured in a field of 50 T presented in Fig. 14, where the shape of the curve becomes asymmetrical and the maximum becomes less pronounced.

Data given in Table 6 compare the maximum values of adiabatic temperature change (ΔT_{ad}) of Dy near its Néel temperature, which were obtained in Refs. [6,8,9,41] and in the present study. It is obvious that the maximum values of ΔT_{ad} are observed for single crystals along the easy magnetization direction (in this case, the easy magnetization axis coincides in the a crystallographic axis [43,44]). It is known that Dy is characterized by high magnetic anisotropy energy [43]. The anisotropy of magnetocaloric effect was studied in Ref. [6]. Studies of the MCE of Dy single crystal in Ref. [6] were fulfilled by direct method in magnetic fields of to 6 T along different crystallographic directions, i.e., ΔT_{ad} was measured over the wide temperature range in magnetic fields of 1, 2, 3, 4, 5, and 6 T along the a and b axes lying in the basal plane. The maximum ΔT_{ad} values were observed near the Néel temperature, which are 6 and 5.2 K along the a and b axes in a field of 5 T, respectively. Thus, it was shown that the difference between ΔT_{ad} measured along the a and b axis near the Néel temperature can reach 0.8 K in a field of 5 T. The higher ΔT_{ad} values a Dy single crystal were obtained in Ref. [41] by calculations using the heat capacity data measured in a magnetic field (indirect method). In this case, ΔT_{ad} was 9 K in a field of 5 T applied along the a axis.

The samples investigated in the present study are polycrystalline fine-grained; they consist mainly of coarse crystallites oriented randomly. In this case, the MCE is determined as the sum of magnetocaloric effects of individual grains (in our case, crystallites) differing the orientation relative to the magnetic field direction. Because of this, the MCE of polycrystalline sample should be lower than that of single crystals. As is seen from Table 6, the values of ΔT_{ad} measured for sublimed Dy in steady magnetic fields agree well with those obtained previously for polycrystalline samples [9,41]. In turn, the values of ΔT_{ad} measured in this work for polycrystalline sublimed Dy, despite the misorientation of individual grains, are comparable with those observed for the single crystals along their a axis in magnetic fields up to 5 T. This indicates the fact that the values of MCE of Dy are mainly determined by its purity since the values observed for single-crystal and polycrystalline samples are comparable. Earlier, this fact was demonstrated for Gd [7].

The used vacuum sublimation is more cost-effective procedure as compared to the single-crystal growth process, has technological advantages, and can be used for creation of REM-based magnetocaloric materials with high values of magnetocaloric parameters.

4. Conclusions

Studies of the MCE in high steady and high pulsed magnetic fields were performed using sublimed high-purity Dy; the polycrystalline structure is formed by coarse crystallites consisting of fine grains. For the first time, the impurity composition of sublimed Dy was characterized in

Table 5
Chemical composition (at %) of the studied samples determined by atom probe tomography.

Sample no.	Fe	C	P	O	Dy	Ho	F	Y	Number of atoms, x10 ⁶
1	0.019	0.0041	0.004	0.66	99.03	0.035	0.26	0.007	1.27
2	0.031	0.0078	0.016	1.81	97.05	0.036	0.12	0.011	1.70

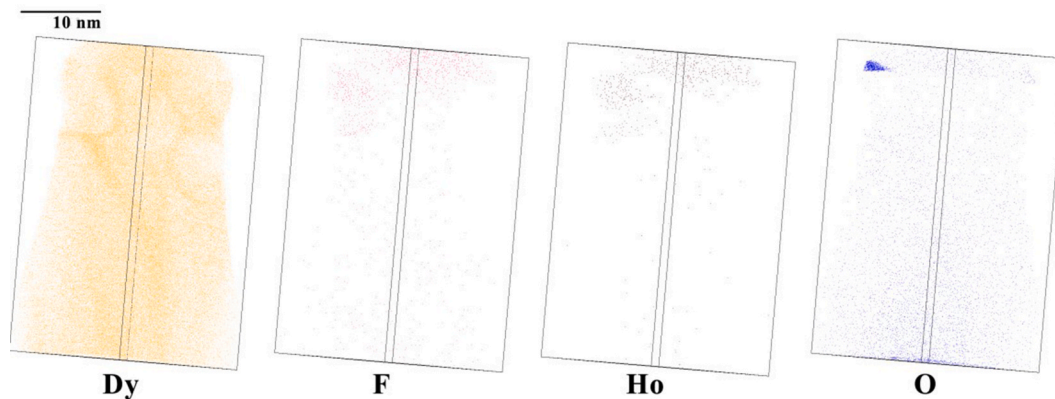


Fig. 8. Atom maps of the dysprosium specimen.

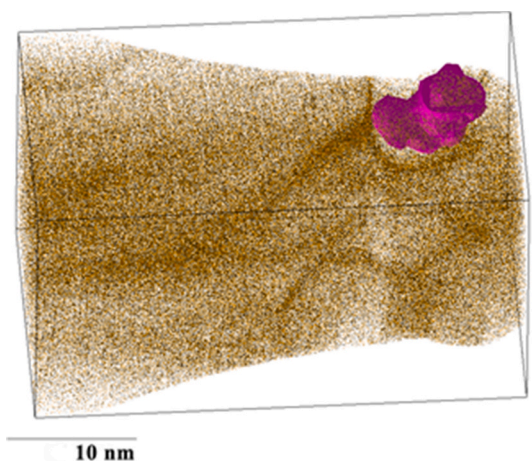


Fig. 9. Isosurface of F-enriched cluster in purple surrounded by Dy atoms (are shown with brown).

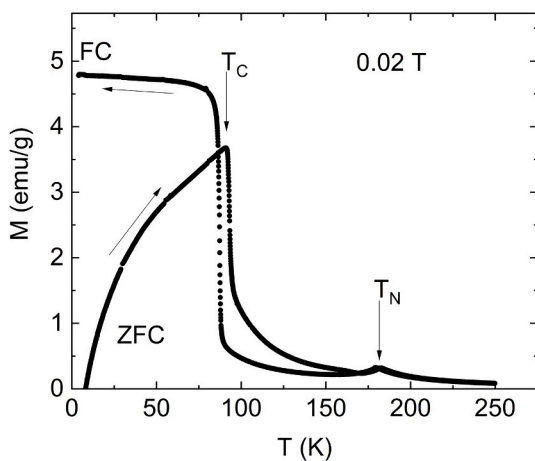


Fig. 10. Temperature dependences of the magnetization of sublimed Dy measure under ZFC and FC conditions in a field of 200 Oe.

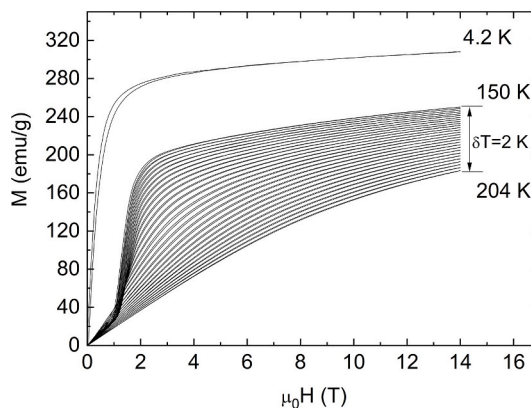


Fig. 11. Magnetization isotherms of sublimed Dy measured at different temperatures.

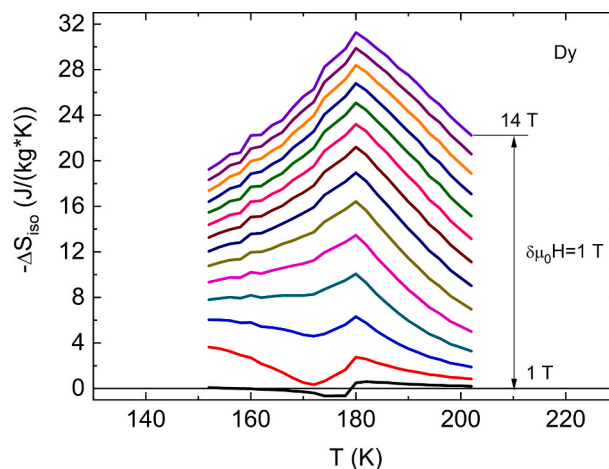


Fig. 12. Temperature dependences of the isothermal entropy change of sublimed Dy (there is 1 T between curves) determined by Eq. (1) using magnetization data in (Fig. 11).

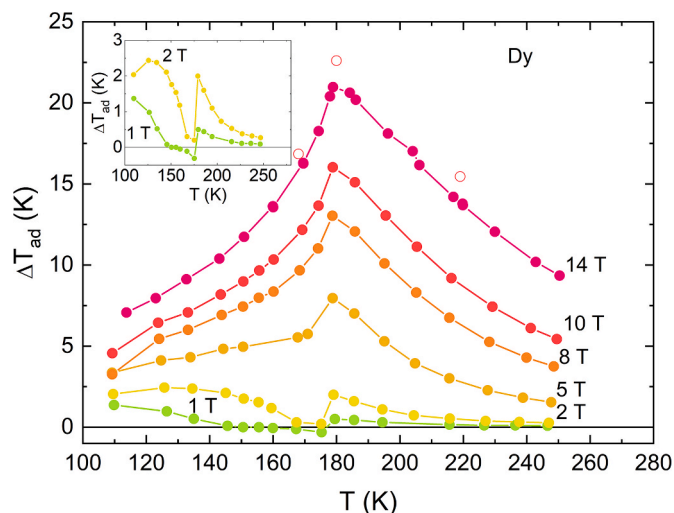


Fig. 13. Temperature dependences of adiabatic temperature change measured by direct method in steady field up to 14 T. Open symbols indicate values obtained in a pulsed magnetic field of 14 T. Inset shows the results for 1 and 2 T.

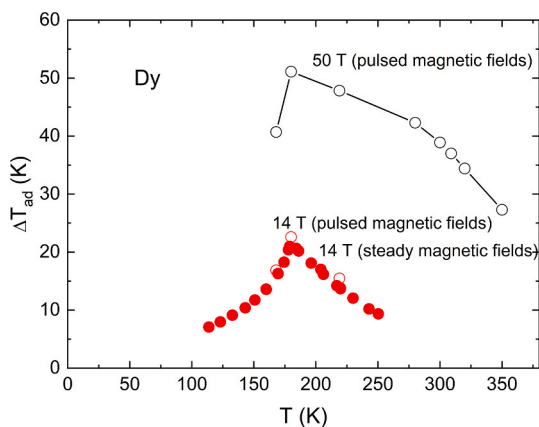


Fig. 14. Temperature dependences of MCE (ΔT_{ad}) for sublimed Dy measured in steady fields of 14 T and pulsed magnetic fields of 14 and 50 T (open symbols).

Table 6

Maximum adiabatic temperature change (ΔT_{ad}) of Dy near the Néel temperature (179 K) determined by direct measurements and calculations for magnetic fields 2, 5 and 10 T.

ΔT_{ad} (K)			Sample/Magnetic field direction	Method (type of magnetic field)	Ref.
$\mu_0 H = 2$ T	$\mu_0 H = 5$ T	$\mu_0 H = 10$ T			
2.2	–	–	polycrystal	Direct	[9]
2.3	8.2	–	polycrystal	Direct	[41]
1.5	6	–	Single crystal/H a	Direct	[6]
1	5.2	–	Single crystal/H b		
2.3	9	19.5	Single crystal/H a	Calculated from heat capacity data	[8]
2	8	16	Sublimed nano-structured	Direct (steady)	This work

detail by atom probe tomography used along with the traditional analytical techniques. The peculiarities of impurity distribution are shown to be related to the behavior of impurities in the course of sublimation, which is in accordance with the vapor pressure of evaporated elements.

The sublimed metal is characterized by presence of nano-sized grains that form crystallites. The texture of crystallites is represented by dominant (67 %) texture-less component.

The MCE of sublimed Dy was studied using direct measurements of the adiabatic temperature change ΔT_{ad} in pulsed (up to 50 T) and steady (up to 14 T) magnetic fields. The maximum value of ΔT_{ad} is observed in the region of the Néel temperature (179 K) and is 22 K in a steady field of 14 T and 51 K in a pulsed magnetic field of 50 T. In a pulsed field of 50 T, the values of ΔT_{ad} of Dy and Gd becomes comparable. The observed experimental fact was theoretically substantiated in Ref. [11] – the ultimate value of ΔT_{ad} at the magnetic phase transformation temperature according to the mean-field model (T_N for Dy and T_C for Gd) is 231 K and 235 K, respectively [11]. The values of ΔT_{ad} obtained for high-purity sublimed Dy are comparable with those obtained for single-crystal Dy in magnetic fields up to 5 T. The realization of high MCE values in sublimed Dy, which are comparable with those for Dy single-crystals and technological advantages of sublimation and distillation manufacturing processes of Dy as well make the sublimed Dy a promising magnetocaloric material for the magnetic refrigeration technology.

CRediT authorship contribution statement

Yu.S. Koshkidko: Writing – review & editing, Writing – original draft, Investigation, Conceptualization. **J. Cwik:** Investigation. **C. Salazar Mejia:** Writing – review & editing, Investigation. **N.A. Dormidontov:** Investigation. **P.A. Prokofev:** Investigation. **A.S. Bakulina:** Investigation. **A.A. Nikitin:** Investigation. **A.A. Khomich:** Investigation. **R.R. Gimaev:** Investigation. **A.S. Andreenko:** Investigation. **Zh.P. Burmii:** Investigation. **A.A. Telitsa:** Investigation. **V.I. Zverev:** Writing – review & editing, Investigation. **N.B. Kolchugina:** Writing – review & editing, Methodology, Investigation, Conceptualization.

Declaration of competing interest

The authors declare that they have no known competing financial interests or personal relationships that could have appeared to influence the work reported in this paper.

Data availability

Data will be made available on request.

Acknowledgments

This work was supported by HLD-HZDR, member of the European Magnetic Field Laboratory (EMFL) and by the Ministry of Education and Science, Poland (grant no. DIR/WK/2018/07) via its membership to the EMFL. The study was performed in terms of state assignment no. 075-01176-23-00. A.S. Andreenko thanks financial support in term of Agreement no. 075-11-2022-013 (5 April 2022) between Kazan' Plant Elektropribor and Physical Faculty of the Moscow State University. The tomographic atom probe, SEM and AFM analysis was carried out using the equipment provided by the KAMIKS Research Equipment Sharing Center (<http://kamiks.itep.ru/>) of the National Research Center Kurchatov Institute.

References

- [1] A.M. Tishin, Y.I. Spichkin, *The Magnetocaloric Effect and its Applications*, CRC Press, 2003.
- [2] K.A. Gschneidner Jr., V.K. Pecharsky, A.O. Tsokol, Recent developments in magnetocaloric materials, *Rep. Prog. Phys.* 68 (2005) 1479, <https://doi.org/10.1088/0034-4885/68/6/R04>.
- [3] S.A. Nikitin, *Magnetic Properties of Rare Earth Metals and Their Alloys*, MSU, 1989 (In Russ.).
- [4] A.S. Andreenko, K.P. Belov, S.A. Nikitin, A.M. Tishin, Magnetocaloric effects in rare-earth magnetic materials, *Sov. Phys. Usp.* 32 (1989) 649, <https://doi.org/10.1070/PU1989v032n08ABEH002745>.

- [5] V.V. Khovaylo, S.V. Taskaev, Magnetic refrigeration: from theory to applications, in: A.-G. Olabi (Ed.), *Encyclopedia of Smart Materials*, Elsevier, Oxford, 2022, pp. 407–417, <https://doi.org/10.1016/B978-0-12-815732-9.00132-7>.
- [6] S.A. Nikitin, A.M. Tishin, P.I. Leontiev, Magnetocaloric effect and pressure influence on dysprosium single crystal magnetization in the range of magnetic phase transition, *J. Magn. Magn. Mater.* 92 (1991) 405–416, [https://doi.org/10.1016/0304-8853\(91\)90855-5](https://doi.org/10.1016/0304-8853(91)90855-5).
- [7] S.Yu Dan'kov, A.M. Tishin, V.K. Pecharsky, K.A. Gschneidner, Magnetic phase transitions and the magnetothermal properties of gadolinium, *Phys. Rev. B* 57 (1998) 3478–3490, <https://doi.org/10.1103/PhysRevB.57.3478>.
- [8] A.S. Chernyshov, A.O. Tsokol, A.M. Tishin, K.A. Gschneidner, V.K. Pecharsky, Magnetic and magnetocaloric properties and the magnetic phase diagram of single-crystal dysprosium, *Phys. Rev. B* 71 (2005) 184410, <https://doi.org/10.1103/PhysRevB.71.184410>.
- [9] A.C. Hudgins, A.S. Pavlovic, Magnetocaloric effect in dysprosium, *J. Appl. Phys.* 36 (1965) 3628–3631, <https://doi.org/10.1063/1.1703055>.
- [10] V.I. Zverev, R.R. Gimaev, A.S. Komlev, B.B. Kovalev, F.G. Queiroz, V.D. Mello, Magnetic properties of dysprosium – experiment and modeling, *J. Magn. Magn. Mater.* 524 (2021) 167593, <https://doi.org/10.1016/j.jmmm.2020.167593>.
- [11] A.M. Tishin, Magnetocaloric effect in strong magnetic fields, *Cryogenics* 30 (1990) 127–136, [https://doi.org/10.1016/0011-2275\(90\)90258-E](https://doi.org/10.1016/0011-2275(90)90258-E).
- [12] M.D. Kuz'min, A.M. Tishin, Magnetocaloric effect Part 2: magnetocaloric effect in heavy rare earth metals and their alloys and application to magnetic refrigeration, *Cryogenics* 33 (1993) 868–882, [https://doi.org/10.1016/0011-2275\(93\)90101-S](https://doi.org/10.1016/0011-2275(93)90101-S).
- [13] F. Willis, N. Ali, Evidence of the c-axis magnetic moment in single-crystal Dy, *J. Appl. Phys.* 69 (1991) 5694–5696, <https://doi.org/10.1063/1.347914>.
- [14] A.S. Chernyshov, A.M. Tishin, K.A. Gschneidner Jr., A.O. Pecharsky, V. K. Pecharsky, T.A. Lograsso, Magnetothermal properties of single crystal dysprosium, *AIP Conf. Proc.* 614 (2002) 19–26, <https://doi.org/10.1063/1.1472521>.
- [15] S.Y. Dan'kov, Yu.I. Spichkin, A.M. Tishin, Magnetic entropy and phase transitions in Gd, Tb, Dy and Ho, *J. Magn. Magn. Mater.* 152 (1996) 208–212, [https://doi.org/10.1016/0304-8853\(95\)00427-0](https://doi.org/10.1016/0304-8853(95)00427-0).
- [16] J. Yu, P.R. LeClair, G.J. Mankey, J.L. Robertson, M.L. Crow, W. Tian, Exploring the magnetic phase diagram of dysprosium with neutron diffraction, *Phys. Rev. B* 91 (2015) 014404, <https://doi.org/10.1103/PhysRevB.91.014404>.
- [17] G.S. Burkhanov, V.B. Chzhan, G.A. Politova, J. Cwik, N.B. Kolchugina, I. S. Tereshina, Multifunctional phenomena in sublimed dysprosium in high magnetic fields: the magnetocaloric effect and magnetostriction, *Dokl. Phys.* 61 (2016) 168–171, <https://doi.org/10.1134/S1028335816040091>.
- [18] V.V. Vorob, M.Ya. Krupotkin, V.A. Finkel, Features of the thermodynamic properties of dysprosium as a quasi-two-dimensional magnetic system, *J. Exp. Theor. Phys. Lett.* 57 (1983) 117.
- [19] V.V. Vorob, M.Y. Krupotkin, V.A. Finkel, Magnetic phase transitions in dysprosium single crystals in weak magnetic fields, *Sov. Phys. JETP* 61 (1988) 1056–1059.
- [20] H.U. Astrom, G. Benediktsson, Magnetic transitions in dysprosium: a calorimetric study, *J. Phys. F Met. Phys.* 18 (1988) 2113–2120, <https://doi.org/10.1088/0305-4608/18/9/028>.
- [21] R. Herz, H. Kronmüller, Field-induced magnetic phase transitions in dysprosium, *J. Magn. Magn. Mater.* 9 (1978) 273–275, [https://doi.org/10.1016/0304-8853\(78\)90069-0](https://doi.org/10.1016/0304-8853(78)90069-0).
- [22] A.S. Chernyshov, Ya Mudryk, V.K. Pecharsky, K.A. Gschneidner, Temperature and magnetic field-dependent x-ray powder diffraction study of dysprosium, *Phys. Rev. B* 77 (2008) 094132, <https://doi.org/10.1103/PhysRevB.77.094132>.
- [23] V.V. Druzhinin, V.M. Melnikov, V.V. Shkarubskiy, Magnetocaloric effect in strong magnetic fields, *Fizika tverdogo tela, Phys. Solid State* 6 (1979) 1750–1753 (In Russ.).
- [24] Y. Waseda, M. Isshiki, *Purification Process and Characterization of Ultra High Purity Metals: Application of Basic Science to Metallurgical Processing*, Springer Berlin Heidelberg, 2012.
- [25] X. Zhang, R. Miao, C. Li, D. Wu, H. Yan, Z. Wang, D. Chen, S. Yan, Z. Li, Impurity distribution in metallic dysprosium during distillation purification, *J. Rare Earths* 34 (2016) 924–930, [https://doi.org/10.1016/S1002-0721\(16\)60116-3](https://doi.org/10.1016/S1002-0721(16)60116-3).
- [26] G. Li, L. Li, R. Miao, W. Tian, S. Yan, X. Li, Research on the removal of impurity elements during ultra-high purification process of terbium, *Vacuum* 125 (2016) 21–25, <https://doi.org/10.1016/j.vacuum.2015.12.003>.
- [27] J. Wang, K. Fu, X. Li, G. Li, Behavior of impurity elements in pure gadolinium during ultra-high purification, *Vacuum* 162 (2019) 67–71, <https://doi.org/10.1016/j.vacuum.2019.01.007>.
- [28] L. Zhang, X. Zhang, Z. Li, S. Pang, Z. Wang, D. Chen, D. Wu, B. Yang, Distribution model of highly volatile impurity in distillate of rare earth metal, *Vacuum* 176 (2020) 109307, <https://doi.org/10.1016/j.vacuum.2020.109307>.
- [29] G.G. Deviatykh, G.S. Burkhanov, *High-Purity Refractory and Rare Metals*, Cambridge International Science Publishing Ltd, Cambridge, 1997.
- [30] S.V. Rogozhkin, A.A. Lukyanchuk, O.A. Raznitsyn, A.S. Shutov, A.A. Nikitin, A. A. Khomich, N.A. Iskandarov, Atom probe tomography analysis of materials using femtosecond-laser assisted evaporation, *J. Surf. Investig.* 12 (2018) 452–459, <https://doi.org/10.1134/S1027451018030175>.
- [31] M.K. Miller, K.F. Russell, Atom probe specimen preparation with a dual beam SEM/FIB miller, *Ultramicroscopy* 107 (2007) 761–766, <https://doi.org/10.1016/j.ultramicro.2007.02.023>.
- [32] V.I. Savyolova, S.F. Kurtasov, T.I. Savyolova, Pole figure measurement plan influence on accuracy ODF coefficients determined by modified harmonic method, *Mater. Sci. Forum* 495–497 (2005) 1693, <https://doi.org/10.4028/www.scientific.net/MSF.495-497.1693>.
- [33] V.N. Serebryany, A.S. Kolyanova, Restoration of the orientation distribution functions from direct polar figures using superposition of normal distributions and arbitrarily defined cells (comparative analysis), *Industrial laboratory, Diagnostic of materials.* 86 (2020) 37–44, <https://doi.org/10.26896/1028-6861-2020-86-9-37-44> (In Russ).
- [34] T.I. Savyolova, S.F. Kurtasov, ODF restoration by orientations grid, *Mater. Sci. Forum* 495–497 (2005) 301–306, <https://doi.org/10.4028/www.scientific.net/MSF.495-497.301>.
- [35] A.S. Kolyanova, V.N. Yaltsev, Misorientation distribution function for cubic crystals, *Industrial laboratory, Diagnostic of materials.* 85 (2019) 28–32, <https://doi.org/10.26896/1028-6861-2019-85-5-28-32> (In Russ).
- [36] S.F. Kurtasov, Method for quantitative analysis of rolling textures of materials with cubic crystal symmetry, *Industrial laboratory. Diagnostic of materials.* 73 (2007) 41–44 (In Russ).
- [37] Y.S. Koshkid'ko, J. Cwik, T.I. Ivanova, S.A. Nikitin, M. Miller, K. Rogacki, Magnetocaloric properties of Gd in fields up to 14T, *J. Magn. Magn. Mater.* 433 (2017) 234–238, <https://doi.org/10.1016/j.jmmm.2017.03.027>.
- [38] C. Salazar Mejía, T. Niehoff, M. Straßheim, E. Bykov, Y. Skourski, J. Wosnitza, T. Gottschall, On the high-field characterization of magnetocaloric materials using pulsed magnetic fields, *J. Phys.: Energy* 5 (2023) 034006, <https://doi.org/10.1088/2515-7655/acd47d>.
- [39] W.C. Koehler, Magnetic properties of rare-earth metals and alloys, *J. Appl. Phys.* 36 (1965) 1078–1087, <https://doi.org/10.1063/1.1714108>.
- [40] M.K. Wilkinson, W.C. Koehler, E.O. Wollan, J.W. Cable, Neutron diffraction investigation of magnetic ordering in dysprosium, *J. Appl. Phys.* 32 (1961) S48–S49, <https://doi.org/10.1063/1.2000493>.
- [41] S.M. Benford, The magnetocaloric effect in dysprosium, *J. Appl. Phys.* 50 (1979) 1868–1870, <https://doi.org/10.1063/1.327148>.
- [42] T. Gottschall, M.D. Kuz'min, K.P. Skokov, Y. Skourski, M. Fries, O. Gutfleisch, M. G. Zavareh, D.L. Schlagel, Y. Mudryk, V. Pecharsky, J. Wosnitza, Magnetocaloric effect of gadolinium in high magnetic fields, *Phys. Rev. B* 99 (2019) 134429, <https://doi.org/10.1103/PhysRevB.99.134429>.
- [43] J.J. Rhyne, A.E. Clark, Magnetic anisotropy of terbium and dysprosium, *J. Appl. Phys.* 38 (1967) 1379–1380, <https://doi.org/10.1063/1.1709631>.
- [44] R.R. Gimaev, A.S. Komlev, A.S. Davydov, B.B. Kovalev, V.I. Zverev, Magnetic and electronic properties of heavy lanthanides (Gd, Tb, Dy, Er, Ho, Tm), *Crystals* 11 (2021) 82, <https://doi.org/10.3390/cryst11020082>.